Digest Journal of Nanomaterials and Biostructures Vol. 20, No. 4, October-December 2025, p. 1475-1485

Effect of copper doping on the optical and structural characteristics of α-Fe_2O_3 thin films fabricated via spray pyrolysis

A . Chibani [a,b], I. Kemerchou [c,*], B . Benhaoua [b], D. Kendil [d]
[a] *Laboratoire Laboratoire revêtement, matériaux et environnement, Boumerdes-University, 35000, Algeria*
[b] *Lab. VTRS, Faculty of Technology, Univ. El-Oued, El oued 39000, Algeria*
[c] *Applied Mechanics and Energy Systems Laboratoty (LMASE), Faculty of Applied Science, University of Ouargla, 30000, Algeria*
[d] *Laboratoire Des Systemes Integres A Base de Capteurs (LSIC), Ecole Normale Supérieure – Kouba16000, Algeria*

Iron(III) oxide (α-Fe_2O_3) is one of the most commonly used metal oxides owing to its excellent chemical stability, abundance, and diverse applications in environmental and industrial technologies. However, its structural and optical properties can be significantly altered depending on the synthesis method and doping concentration. The present work examines the impact of introducing copper dopants on the structural and optical behaviour of α-Fe_2O_3 thin film. The thin films were fabricated via the spray pyrolysis technique with copper doping concentrations of 2%, 4%, 6%, 8%, and 10%. X-ray diffraction (XRD) analysis verified the successful formation of the rhombohedral α-Fe_2O_3 phase, exhibiting a strong preferred orientation along the (110) plane. A shift in the diffraction peaks toward higher angles, along with the emergence of additional peaks at higher doping levels, indicated structural modifications due to copper incorporation.Optical characterisation using UV-Vis spectroscopy in the 300–850 nm range revealed that the doped films exhibit high transparency, reaching up to 90%. Moreover, A noticeable reduction in the direct optical band gap was observed, decreasing from 2.38 eV to 2.19 eV with increasing Cu concentration. These results demonstrate the enhanced potential of copper-doped α-Fe_2O_3 films for applications in optoelectronic and photovoltaic devices.

(Received July 26, 2025; Accepted November 20, 2025)

Keywords: Cu-Fe_2O_3, Spray pyrolysis, UV-Vis, XRD, Thin films

1. Introduction

Metal oxides belonging to the family of transparent and conductive oxides (TCO) are multifunctional materials with remarkable optoelectronic properties. These materials have attracted significant attention for their applications in solar cells, smart windows, sensors, and photocatalysis. Among them, iron oxides stand out due to their low cost, chemical stability, environmental compatibility, and broad applicability. In this work, iron was selected as the base element, and we aim to investigate the optical properties of its oxides through the fabrication and characterization of thin films, with a particular focus on the enhancement provided by copper doping. The films were deposited using spray pyrolysis, a versatile and scalable technique known for its simplicity and cost-effectiveness [1].

Iron exists in various forms in nature, including oxides, hydroxides, and oxyhydroxides, and plays essential roles in both geological and biological systems. It is found in ores, soils, and biological components, such as hemoglobin. Iron compounds are also widely utilised in metallurgy, pigments, catalysis, and magnetic devices [2].

Iron oxides, such as hematite , maghemite, and magnetite , are polymorphic forms with distinct structural and magnetic behaviours. These materials have been historically used in pigments,

* Corresponding author: kemerchou.imad@univ-ouargla.dz
https://doi.org/10.15251/DJNB.2025.204.1475

especially in prehistoric cave paintings. Today, they are applied in diverse areas of science and technology, including environmental remediation, corrosion protection, and biomedical engineering [3].

Iron oxide pigments are valued in the coatings, ceramics, glass, and polymer industries due to their non-toxic and stable nature. Naturally occurring iron oxides represent over 5% of the Earth's crust. They differ in iron oxidation states, chemical composition, and crystal structure. Polymorphs are typically designated by Greek letters such as α, β, and γ [4]. The development of thin film materials is crucial in modern technologies. Iron oxide thin films have shown promise for applications in photoelectrochemical cells and environmental sensors. Their properties are significantly influenced by fabrication parameters such as doping concentration, substrate temperature, and spray rate. copper-doped α-Fe_2O_3 thin films, in particular, the materials show improved charge carrier separation and enhanced absorption in the visible region, thereby increasing their potential for photocatalytic use. [5].

In this study, undoped and Cu-doped α-Fe_2O_3 thin films were synthesised via the spray pyrolysis technique. The impact of copper incorporation on their structural and optical characteristics was thoroughly investigated using various characterisation methods, including X-ray diffraction (XRD) and UV–Vis spectroscopy. Our objective is to optimise doping levels to improve film transparency and photocatalytic performance. Iron oxide-based materials have been successfully applied in catalysis [6], soil remediation [7], and antibacterial coatings [8].

Furthermore, iron oxide nanoparticles have increasingly drawn attention for environmental cleanup applications due to their large surface area, notable magnetic properties, and high chemical reactivity[9,10].

2. Materials and methods

2.1. Thin films preparation

To develop α- Fe_2O_3 iron oxide, a doped solution with (2, 4, 6, 8, and 10wt) Cu/Fe was used in the deposition of α-Fe_2O_3 thin layers by SPMN, where iron chloride powder ($FeCl_3$) at a molar concentration of (0.25 mol/l) was used.The weighed quantities of ($FeCl_3$) are then dissolved in of 50 ml at ratio of 1:1 volume methanol and distilled water The obtained blend solution was stirred for 45 minutes by magnetic stirrer until complete dissolution (brownish-red solution). In order to prepare the ion copper (Cu^{2+}) solution, the same process was proceeded as in preparing the pure iron ionic solution. The volume of 50 ml of dissolved iron solution is divided into 6 equal volumes (volume of 8 ml). Amounts of copper chloride solution according to the doping rates (2, 4, 6, 8 and 10% Cu/Fe) are added to each 8ml mixture mother solution as described in the following table.

Table 1. The volumetric doping ratios along with the volume of the copper solution.

Doping (% Cu/Fe)	2	4	6	8	10
V"(ml) Cu	**0.16**	**0.32**	**0.48**	**0.64**	**0.8**

where V": volume of copper chloride $CuCl_2$ solution.

Thin films with Cu doping levels of 2%, 4%, 6%, 8%, and 10% were fabricated by spraying each solution separately.

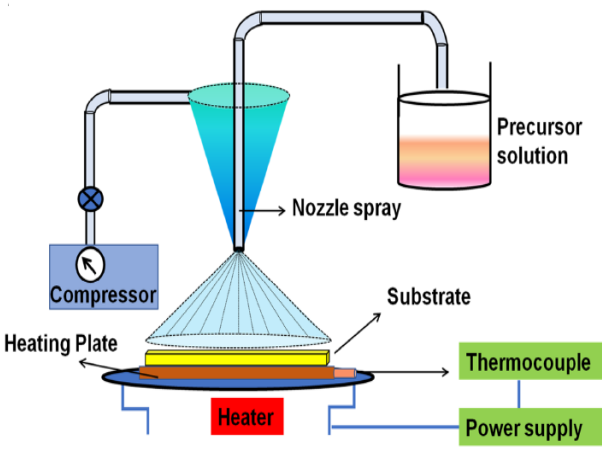

Fig. 2. Deposition of Thin Films Using the Moving Nozzle Spray Pyrolysis Method (SPMN) [10].

2.2. Thin Film Analysis

The crystallographic structure of Cu-doped α-Fe_2O_3 thin films with doping concentrations ranging from 0% to 10% was characterised using a Philips X-ray diffractometer. The optical behaviour, including transmittance and band gap energy, was examined with a Shimadzu UV–VIS spectrophotometer in the wavelength range of 300–900 nm. Furthermore, Fourier Transform Infrared (FT-IR) spectroscopy was carried out using a Shimadzu IR-Infinity 1 spectrometer over the spectral range of 400–4000 cm^{-1}. All characterisation analyses were performed at room temperature

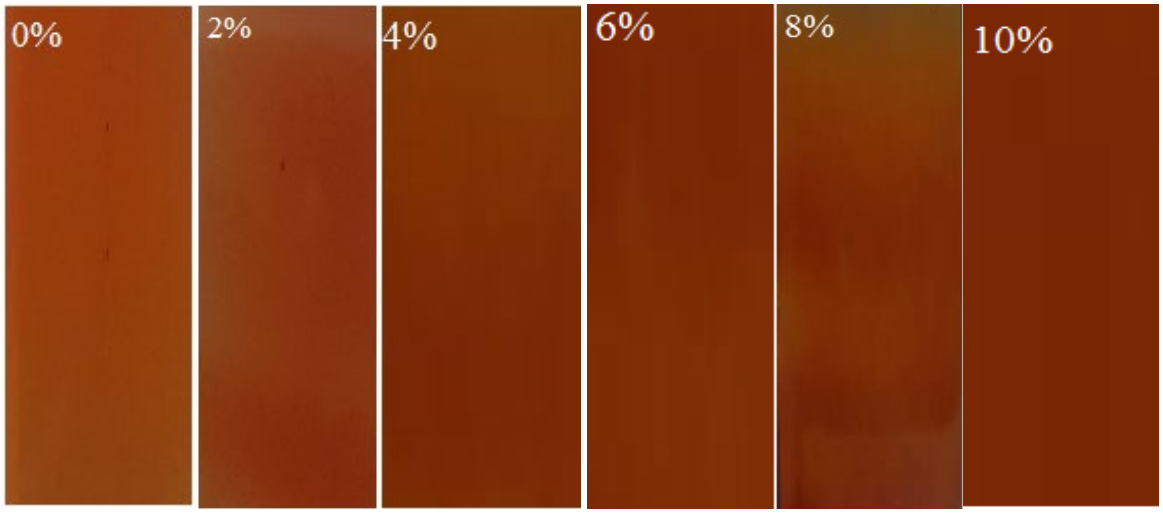

Fig. 3. Photographic images of the synthesised α-Fe_2O_3 *thin films doped with 0–10 % copper.*

3. Analysis and Discussion of Results

After Cu doping at different concentrations, noticeable changes in the film's composition were observed, with certain phases appearing while others disappeared. Consequently, the structural and chemical characteristics of the doped thin films differed significantly from those of the undoped samples

3.1. Structural characterization of α-Fe_2O_3

3.1.1. X-ray diffraction

Figure 4 displays the X-ray diffraction (XRD) patterns of pure and Cu-doped α-Fe_2O_3 thin films prepared with doping concentrations of 0, 2, 4, 6, 8, and 10%. Distinct diffraction peaks were observed at 2θ values of around 29.13°, 32.97°, 35.76°, 41.11°, 49.58°, and 64.22°, which are indexed to the (012), (104), (110), (113), (024), and (300) crystal planes of α-Fe_2O_3, respectively. The presence of these characteristic peaks confirms the successful formation of the rhombohedral hematite phase in all synthesised films.which is in good agreement with the standard reference data reported by the Joint Committee on Powder Diffraction Standards (JCPDS card No. 01-073-2234).

For all Cu-doped samples, the diffraction peaks of the undoped α-Fe_2O_3 phase are retained, indicating that doping does not alter the fundamental crystal structure. However, a noticeable shift of the (110) peak towards higher 2θ values is observed with increasing Cu doping concentration. This peak shift suggests a contraction in the lattice structure, which could be attributed to the substitutional incorporation of Cu^{2+} ions (ionic radius ≈ 0.073 nm) into the Fe^{3+} sites (ionic radius ≈ 0.064 nm). The resulting lattice distortion may induce internal compressive stress within the thin film structure.

In particular, the (110) diffraction peak reaches its highest intensity at 4 % Cu doping, followed by a gradual decrease in intensity at higher doping levels (6% to 10%). This trend indicates a possible optimal crystalline ordering or crystallite growth at this doping level, which becomes disrupted with further increase in dopant content. A similar evolution is observed for other planes such as (104), (214), and (300), especially the (104) peak, which becomes more prominent starting from the 4% doping level and continues to intensify up to 10%.

These observations collectively imply that copper incorporation at appropriate levels can influence the crystal quality and strain state of α-Fe_2O_3 thin films, which is crucial for tuning their physical properties in optoelectronic and catalytic applications

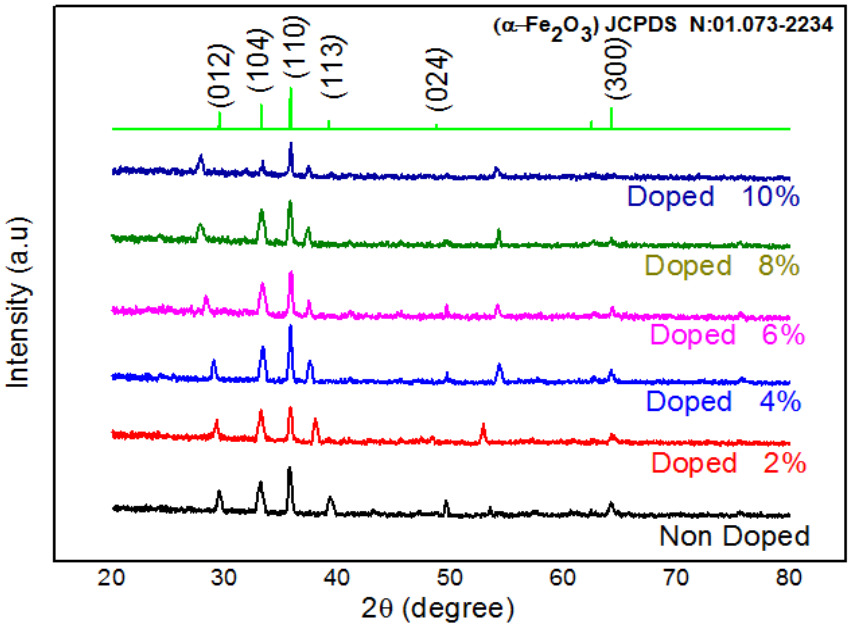

Fig. 4. X ray spectra of 0, 2, 4, 6, 8, and 10% Cu doped α-Fe_2O_3 *thin films.*

3.1.2. Crystallite size

The crystallite size of undoped and Cu-doped α-Fe_2O_3 thin films corresponding to the (110) diffraction plane was quantitatively evaluated from the X-ray diffraction (XRD) patterns using the Debye–Scherrer equation. The obtained values are presented in Table 2, and they fall within the nanometric scale, ranging from 16.14 nm to 33.01 nm, indicating that the prepared films possess a polycrystalline nature. The largest crystallite size was observed at 4 % Cu doping, suggesting enhanced crystallinity at this level, whereas the smallest size was recorded at 10 %, likely due to increased lattice distortion and structural defects at higher doping concentrations.

The determination of the lattice parameters a and c was carried out using HighScore software and compared with the standard values from JCPDS card No. 01-073-2234 (a_0 = 5.032Å, c_0= 13.74 Å). It is evident that for undoped and up to 4% Cu-doped samples, both a and c remain slightly below the standard values. However, for doping levels beyond 4%, the lattice parameters a and c increase progressively, exceeding the standard reference values. This trend confirms the successful substitution or interstitial incorporation of Cu^{2+} ions into the α-Fe_2O_3 lattice, which results in lattice expansion.

The variation in the interplanar spacing d across the (012), (104), and (110) planes further supports this structural evolution. A minor shift in the 2θ angles to higher values, especially in the (110) peak, corresponds to slight lattice compression or distortion, particularly at lower doping levels. As the Cu content increases, the average shift and broadening of peaks suggest higher internal strain and possible dislocation density in the lattice.

In terms of optical properties, the band gap energy was found to vary between 2.14 eV and 2.389 eV, depending on the doping concentration. A decrease in Eg at 4% and 6% doping suggests enhanced electronic transitions and potential for better light absorption, which is desirable in photoelectronic and photocatalytic applications. The slight increase again at 10% may result from quantum confinement effects due to the reduced crystallite size.

Additionally, the decrease in crystallite size observed at certain doping levels (e.g., 6% and 10%) may be attributed to structural disorder caused by the mismatch in ionic radii between Fe^{3+} (~0.064 nm) and Cu^{2+} (~0.073 nm), leading to lattice strain and partial degradation of crystallinity. Conversely, the increase in crystallite size at 4% could be linked to improved atomic arrangement and minimised defect formation.

The lattice parameters a and c for the rhombohedral α-Fe_2O_3 structure were derived using established mathematical relations based on the observed XRD peak positions [11]

$$2d_{hkl}\sin(\theta) = n\lambda \tag{1}$$

and

$$\frac{1}{{d_{hkl}}^2} = \frac{4}{3a^2}(h^2 + k^2 + hk) + \frac{l^2}{c^2} \tag{2}$$

Table 2. Lattice parameters, crystallite seize D and band gap E_g of undoped and Cu doped α-Fe_2O_3 thin films.

Doping (Cu)%	(*hkl*)	2*θ* (°)	Lattice Parameters (Å)		Calculated *d*(Å)	E_g(eV)	Cristallite size *D*(nm)
			a=b	*C*			
Non dope	(*012*)	29.429	5.0246	13.722	3.032	2. 38	31.625
	(*104*)	33.075			2.706		
	(*110*)	35.656			2.516		
2%	(*012*)	29.323	5.0247	13.7332	3.043	2. 30	30.423
	(*104*)	33.181			2.697		
	(*110*)	35.761			2.508		
4%	(*012*)	28.902	5.0281	13.7390	3.677	2.15	33.010
	(*104*)	33.299			2.696		
	(*110*)	35.761			2.514		
6%	(*012*)	28.362	5.0352	13.7550	3.682	2.20	25.190
	(*104*)	33.299			2.700		
	(*110*)	35.761			2.517		
8%	(*012*)	27.823	5.0373	13.7609	3.684	2.14	24.900
	(*104*)	33.181			2.701		
	(*110*)	35.761			2.518		
10%	(*012*)	27.827	5.0378	13.7712	3.685	2.19	16.140
	(*104*)	33.405			2.702		
	(*110*)	35.761			2.518		

Also, The enlargement of the lattice parameters in Cu-doped α-Fe_2O_3 nanoparticles is commonly ascribed to the ionic substitution of Fe^{3+} (0.065 nm) by the relatively larger Cu^{2+} ions (0.073 nm), which induces lattice expansion due to the size mismatch [12].

No additional Cu-related peaks were detected in the XRD patterns; however, a slight shift of diffraction peaks toward lower 2θ values was observed with increasing Cu content. All samples exhibited a main peak at 35.76° corresponding to the (110) plane, while the peak intensity showed minor fluctuations compared to the undoped film, indicating that Cu incorporation affects the crystallinity without changing the phase structure.

As summarised in Table II, the crystallite sizes of thin films with different doping concentrations were estimated from multiple well-defined diffraction peaks, and the average crystallite size was subsequently calculated using the Scherrer equation. [13].

$$D = \frac{0.9\,\lambda}{\beta cos\theta} \tag{3}$$

Here, D, β, λ, and θ represent the crystallite size, FWHM, X-ray wavelength (1.5406 Å), and Bragg angle, respectively[14].

3.2. Optical Properties of Pure and Cu-Doped α-Fe_2O_3 Thin Films

3.2.1. Optical transmittance

Figure 5 illustrates the transmittance spectra of α-Fe_2O_3 thin films doped with 0–10% Cu.The transmittance spectrum of undoped sample was found to be about 65%. An increase in the value of the transmittance for all doped samples (more than 72%). This value increases only more than 90% for 6% which may be related to a feeble energy dispersion because of its structure amelioration (see X-ray diffraction) ted to Cu doped samples with a certain blue shift the later sample (see the green spectrum of Figure 5. For all samples, the transmittance spectra decrease dramatically at waves

lengths below 550 nm, this behaviour is attributed to the fundamental absorption of the material, which is directly related to the optical band gap (Eg) of α-Fe_2O_3 . The Eg values were estimated using Tauc's relation, expressed as follows [10]:

$$(\alpha h\nu)^n = A(h\nu - Eg) \quad (4)$$

where ***A*** is a constant and n is taken 2 based on the fact that α-Fe_2O_3 has an direct gap [15, 16,17]. In (Figure .) show Diffuse transmittance spectra (UV-vis DRS) of undoped and Cu (0-10%) doped α-Fe_2O_3 NPs recorded in the range from 300-800 nm.

The spectral transmittance measurements show that the films were more than 75% transparent in the visible area; a minor reduction was seen with doping. The presence of interference patterns (Figure 5) in the transmittance data (T%) provides direct proof of consistently homogeneous [14]. The absorption coefficient was estimated using Lambert's relation

These values indicate that the α-Fe_2O_3 thin films exhibit notable transparency in the visible region. This high level of transparency is one of the key properties that makes α-Fe_2O_3 thin films attractive for various optical applications [18].

$$\alpha = \ln\left(\frac{1}{T}\right) \quad (5)$$

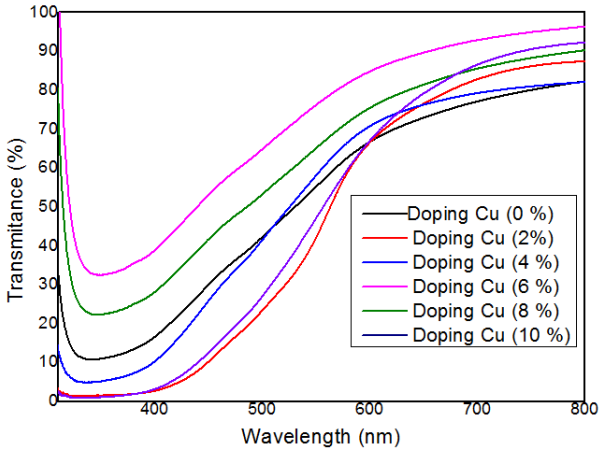

Fig. 5. Transmittance Spectra of Pure and Cu-Doped α-Fe_2O_3 Thin Films.

3.2.2. Optical bandgap calculation

The optical band gap (Eg) for non-doped **α**-Fe_2O_3 thin films is up to 2.38eV, however for high acceptor doped materials, it changes to lower energies (longer wavelengths) in the 2. 30 -2.14 eV range. Figure 6. depicts the results obtained.

Table 3. Urbach energy (Eu) and band gab (Eg) of 0-10% Cu-doped Fe_2O_3 thin films.

Doping (%)	Urbach energy (eV)	Band gab(eV)
0	0.33	2.38
2	0.41	2.30
4	0.73	2.15
6	0.38	2.20
8	0.57	2.14
10	0.20	2.19

The Urbach energy (Eu), which reflects the degree of structural disorder within the thin film matrix, is related to the absorption spectrum according to:

$$\ln \alpha = \alpha_0 + \frac{h\nu}{Eu} \quad (6)$$

Here, α is the absorption coefficient, α_0 a constant, h Planck's constant, ν the incident frequency, and E_u the Urbach energy. E_u was obtained from the inverse slope of the linear plot of ln(α) versus hν. As shown in Table III, E_u increases with Cu doping up to 8% before decreasing at higher levels. Moreover, E_u exhibits an inverse relationship with Eg across the doping range, as illustrated in Figure 6.

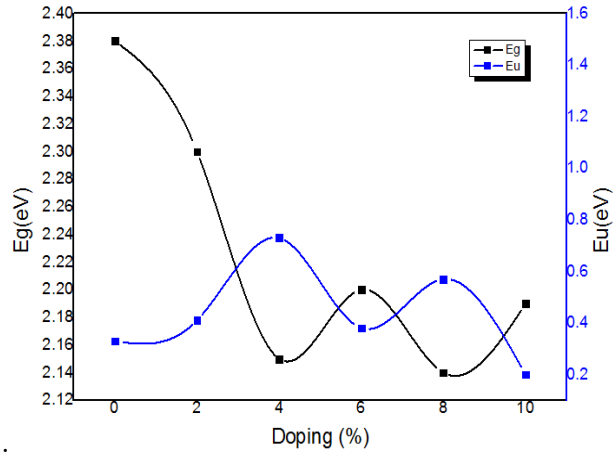

Fig. 6. Optical band gap (Eg) and Urbach energy (Eu) variations for 0-10 % Cu-doped α-Fe_2O_3 thin films.

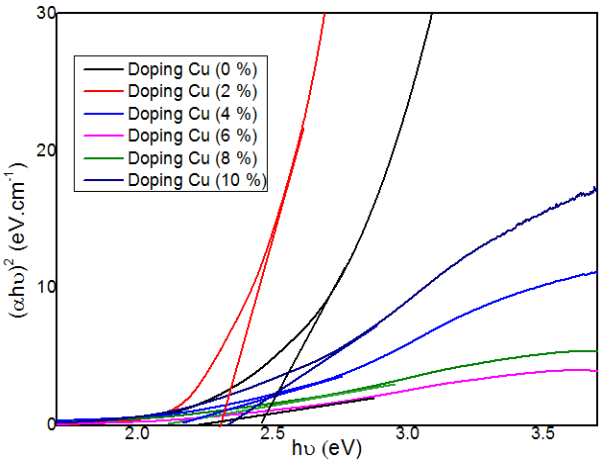

Fig. 7. Optical band gap of (0-10 %) Cu doped α-Fe_2O_3 thin films

3.4. FTIR analysis

The existence of various functional groups of the elaborated 0-10 % Cu-doped Fe_2O_3 thin films may be investigated using FTIR spectroscopy. Figure 8. exhibits the spectra of non and Cu-doped Fe_2O_3. All samples show a high absorption band between 400-500cm^{-1}, indicating a stretching vibration of the Fe-O-Fe link. The relevant literature reported various differences in the location of the typical IR absorption bands associated with the Fe-O-Fe link. At global sight, there were three peaks of absorptions at 400, 640, and 730cm-1 which are assigned to Fe-O-Fe, O-Fe-O and Fe-O. The stretching vibration of the Fe–O–Fe bond shifted to higher wavenumbers after Cu doping, from

400 to 420 cm^{-1} and from 730 to 740 cm^{-1} (Figure 8). This shift is attributed to the substitution of Fe atoms by Cu, which becomes evident after doping. Since Cu atoms (63.54 g/mol) are heavier than Fe (55.84 g/mol), their incorporation leads to absorption at lower frequencies [19], which means heigh waves lengths as it was observed.

The changes observed in the FTIR spectra with increasing Cu doping are mainly due to:

- Substitution of Fe^{3+} by Cu^{2+} ions, leading to lattice distortion.
- Formation of Cu–O bonds and possible surface species, especially around 900 cm^{-1}.
- Increased structural disorder and defects at higher doping levels, causing peak broadening and intensity variation.
- Shift and weakening of Fe–O vibrational bands indicate local strain and changes in crystal symmetry.

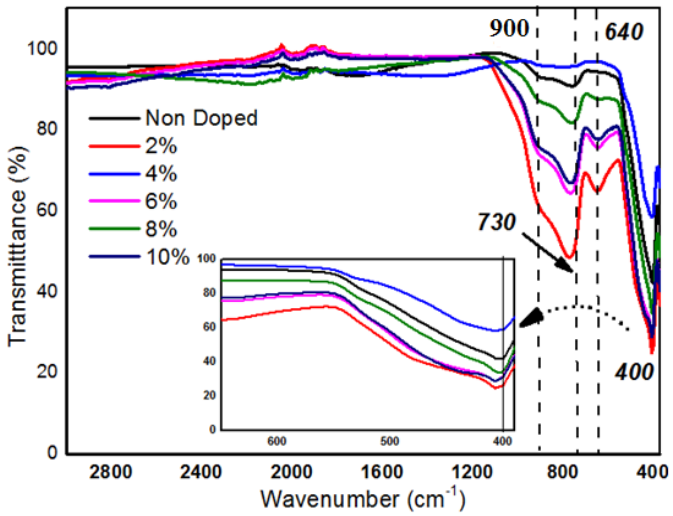

Fig. 8. FTIR Analysis of Pure and Cu-Doped α-Fe_2O_3 Thin Films.

4. Conclusion

In this study, Cu-doped α-Fe_2O_3 thin films with doping levels between 0% and 10% were successfully fabricated via the spray pyrolysis method. Their structural, optical, and vibrational characteristics were comprehensively analysed through X-ray diffraction (XRD), UV–Vis spectroscopy, and (FTIR) spectroscopy.

XRD analysis verified the formation of a rhombohedral hematite crystal structure exhibiting a preferred orientation along the (110) plane. A shift in 2θ values and variation in crystallite sizes (from 16.14 to 33.01 nm) revealed that Cu incorporation alters the lattice, with optimal crystallinity observed at 4% doping. Lattice parameter analysis indicated an increase beyond 4% doping, suggesting successful substitution or interstitial incorporation of Cu^{2+} ions into the Fe_2O_3 matrix.

Optically, the band gap energy varied between 2.14 and 2.38 eV, showing a slight redshift with increasing Cu content, which enhances the films' potential for visible light absorption. FTIR spectra supported the structural findings, with shifts and intensity changes in Fe–O and Cu–O vibrational modes, highlighting increased lattice disorder at higher doping levels.

The FTIR analysis further confirmed the structural modifications induced by Cu doping, as evidenced by the shifts and intensity changes in the Fe–O vibrational bands, indicating successful incorporation of copper into the hematite lattice.

Future Outlook

The tunability of structural and optical properties through controlled Cu doping demonstrates that α-Fe_2O_3 thin films can be tailored for optoelectronic and photocatalytic applications. Future work will focus on evaluating the films' photoelectrochemical performance, stability under solar irradiation, and potential integration into devices such as photoanodes and gas sensors

Acknowledgments

We gratefully acknowledge the support of the Faculty of Technology, El-Oued University

References

[1] Arefi H., Arabi H., Surface and Coatings Technology 462, 129417 (2023).

[2] Saito Y., Yamashita T., Okabe K., Liu J., Advanced Functional Materials 35(7), 2300345 (2025).

[3] D.Bekkar, Y.Meftah, B.Benhaoua, A.Rahal, A.Benhaoua,A..H.Hamzaoui, Journal of Optoelectronic and Biomedical Materials. 33 - 42 (2020); https://doi.org/10.15251/JOBM.2020.122.33

[4] Mauvernay B., Thin Solid Films 783, 139537 (2023).

[5] Mohamed R., El-Wahab A., Kassem H., Scientific Reports 14(1), 1872 (2024).

[6] Zhao L., Wang M., Li H., Journal of Environmental Chemical Engineering 12(3), 109872 (2024).

[7] He S., Feng Y., Ni J., Yu Y., Chemosphere 328, 138593 (2023).

[8] Ubale A., Belkhedkar M., Journal of Biomedical Materials Research 111(4), 1023 (2023).

[9] Akbar A., Yousaf H., Riaz S., Naseem S., Journal of Magnetism and Magnetic Materials 594, 170364 (2025).

[10] A Chibani, D Kendil, B Benhaoua, I Kemerchou, D Bekkare, Digest Journal of Nanomaterials & Biostructures (DJNB)17.4 (2022); https://doi.org/10.15251/DJNB.2022.174.1463

[11] Fu H, Quan X, Zhao H., J Photochem Photobiol Chem,2005, 173: 143; https://doi.org/10.1016/j.jphotochem.2005.01.013

[12] D. K. Kim, M. Mikhaylova, Y. Zhang, M. Muhammed, Chemistry of Materials 15(8), 1617 (2003); https://doi.org/10.1021/cm021349j

[13] F.F.H. Aragón, J.D. Ardisson, J.C.R. Aquino, I. Gonzalez, W.A.A. Macedo, J.A.H. Coaquira, J. Mantilla, S.W. da Silva, P.C. Morais, Thin Solid Films 607, 50. (2016); https://doi.org/10.1016/j.tsf.2016.03.052

[14] Y. Meftah, D. Bekker, B. Benhaoua, A. Rahal, A. Benhaoua, A. Hamzaoui, Digest Journal of Nanomaterials and Biostructures, 13(2), 465 (2018).

[15] E. Vasile, M. Sima, A. Sima, Digest Journal of Nanomaterials and Biostructures vol. 15, no. 3, july - september 2020, p. 699 – 706; https://doi.org/10.15251/DJNB.2020.153.699

[16] Ali Badawi, M. G. Althobaiti, Sami S. Alharthi, Abdulaziz N. Alharbi, Ali A. Alkathiri, Sultan E. Alomairy, Applied Physics A (2022) 128:123; https://doi.org/10.1007/s00339-021-05154-9

[17] Eman. K Tawfik, Wael H.Eisa, N. Okasha, H.A.Ashry, J. Sci. Res. Sci., Vol. (37), 2020; https://doi.org/10.21608/jsrs.2020.129917

[18] I. Kemerchou, F. Rogti, B. Benhaoua, N. Lakhdar, A. Hima, O. Benhaoua, A. Khechekhouche, Journal of Nano- and Electronic Physics, 11(3), 2019

[19] F. Chouikh , Y. Bouznit , N. Mahamdioua , S.P. Altintas, Materials Chemistry and Physics 252 (2020) 123205; https://doi.org/10.1016/j.matchemphys.2020.123205